Cell Reports, Volume *30*

Supplemental Information

Dynamic Interstitial Cell Response during Myocardial Infarction Predicts Resilience to Rupture in Genetically Diverse Mice

Elvira Forte, Daniel A. Skelly, Mandy Chen, Sandra Daigle, Kaesi A. Morelli, Olivia Hon, Vivek M. Philip, Mauro W. Costa, Nadia A. Rosenthal, and Milena B. Furtado

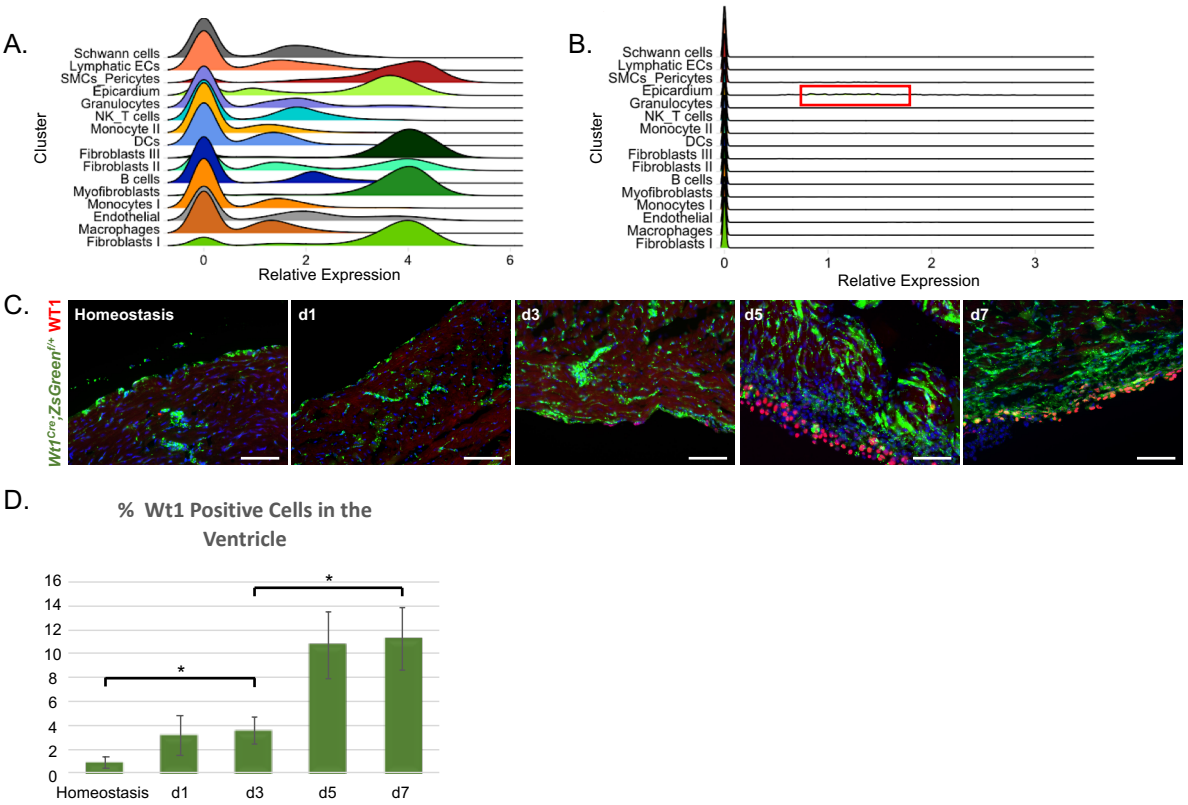

Figure S1 *De novo* expression of *Wt1* in the epicardium post-MI. Related to Figure 1. (*A*) Ridge-plot showing *ZsGreen* mRNA expression in the 16 clusters identified with Seurat from the aggregate of all 7 time-points. High *ZsGreen* levels are seen in smooth muscle cells (SMCs)_Pericytes, epicardium, Fibroblasts type I, II, II and myofibroblasts. (*B*) Ridge-plot showing *Wt1* mRNA expression in all clusters. Note very low detection in the epicardium (red bracket), but no detection in other clusters. (*C*) Immunofluorescent staining for WT1 protein (red) on section of $Wt1^{Cre};ZsGreen^{f/+}$ mouse heart at homeostasis, d1, d3, d5 and d7 post-MI. WT1 is mostly detected in the activated epicardium at d7. (*D*) Quantification of WT1+ cells in the interstitial space of ventricles (n = 6 frames per heart and time-point, including the epicardial region). The statistical significance compared to homeostasis was determined using an unpaired Student's t test ($*p < 0.05$). Scale bar = 50um.

A.

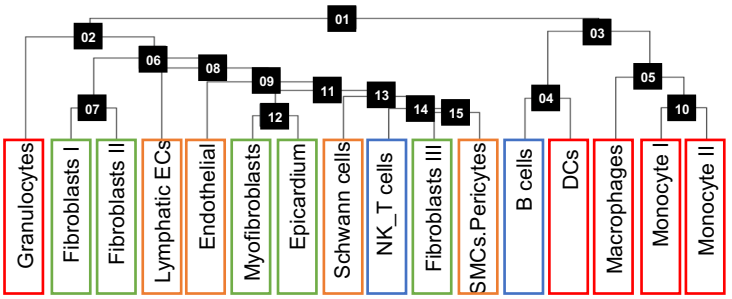

B.

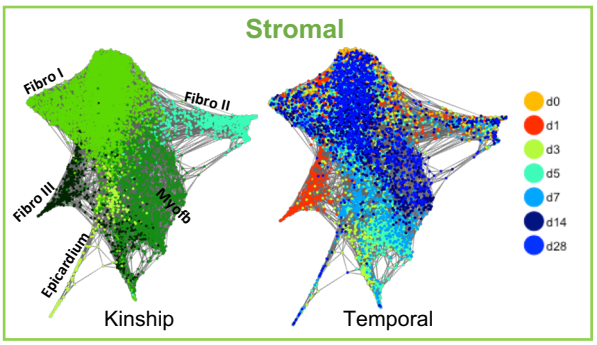

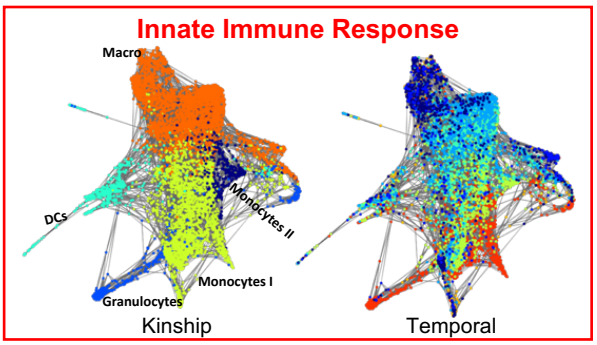

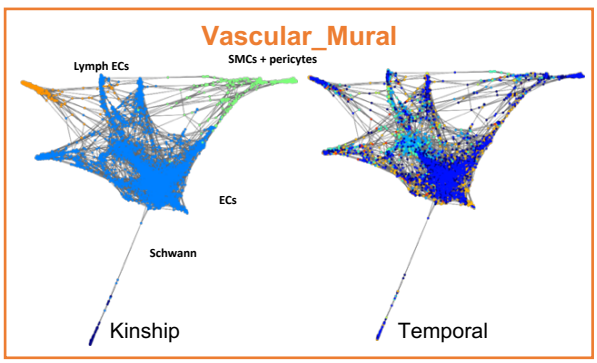

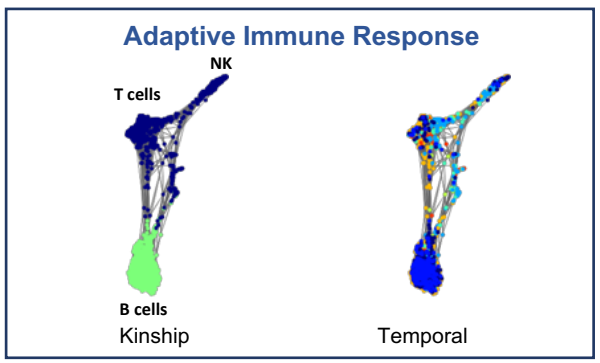

C.

Stromal Cells	https://kleintools.hms.harvard.edu/tools/springViewer_1_6_dev.html?client_datasets/CleanFibro2/CleanFibro2
Innate IR	https://kleintools.hms.harvard.edu/tools/springViewer_1_6_dev.html?client_datasets/InnateIRnew/InnateIRnew
Vascular_Mural	https://kleintools.hms.harvard.edu/tools/springViewer_1_6_dev.html?client_datasets/VascularMural/VascularMural
Adaptive IR	https://kleintools.hms.harvard.edu/tools/springViewer_1_6_dev.html?client_datasets/AdaptiveIR/AdaptiveIR
Day 0	https://kleintools.hms.harvard.edu/tools/springViewer_1_6_dev.html?client_datasets/Day0/Day0
Day 1	https://kleintools.hms.harvard.edu/tools/springViewer_1_6_dev.html?client_datasets/d1/d1
Day 3	https://kleintools.hms.harvard.edu/tools/springViewer_1_6_dev.html?client_datasets/d3/d3
Day 5	https://kleintools.hms.harvard.edu/tools/springViewer_1_6_dev.html?client_datasets/d5/d5
Day 7	https://kleintools.hms.harvard.edu/tools/springViewer_1_6_dev.html?client_datasets/d7/d7
Day 14	https://kleintools.hms.harvard.edu/tools/springViewer_1_6_dev.html?client_datasets/d14/d14
Day 28	https://kleintools.hms.harvard.edu/tools/springViewer_1_6_dev.html?client_datasets/d28/d28

Figure S2 Onset of new populations as a function of the repair process. Related to Figures 1-2. (*A*) Transcriptome based phylogenetic tree of the 16 clusters obtained from the aggregate of interstitial cells derived from *Wt1^{Cre}; ZsGreen$^{f/+}$* mice at homeostasis, d1, d3, d5, d7, d14 and d28 post-MI. Box colors indicate lineage identity (red- innate immune response, blue – adaptive immune response; green – stromal; orange – vascular, mural). (*B*) SPRING k- nearest-neighbor (knn) graphs of cell populations divided by lineage, colored by cluster (Kinship) and time (Temporal). A maximum of 1,200 cells were used in each lineage aggregate per time-point. (C) Links to the SPRING kinetic visualizations for each of the aggregates in (B) and individual time points. The drop-down menu in the website, allows to choose among different types of visualization: “Default”, “Louvain Cluster”, “Type” = clusters defined with Seurat v2, “Time”. For the Stromal cell aggregate “TypeA” indicates the initial clustering (Figure1), “TypeB”, the sub-clusters (Figure2).

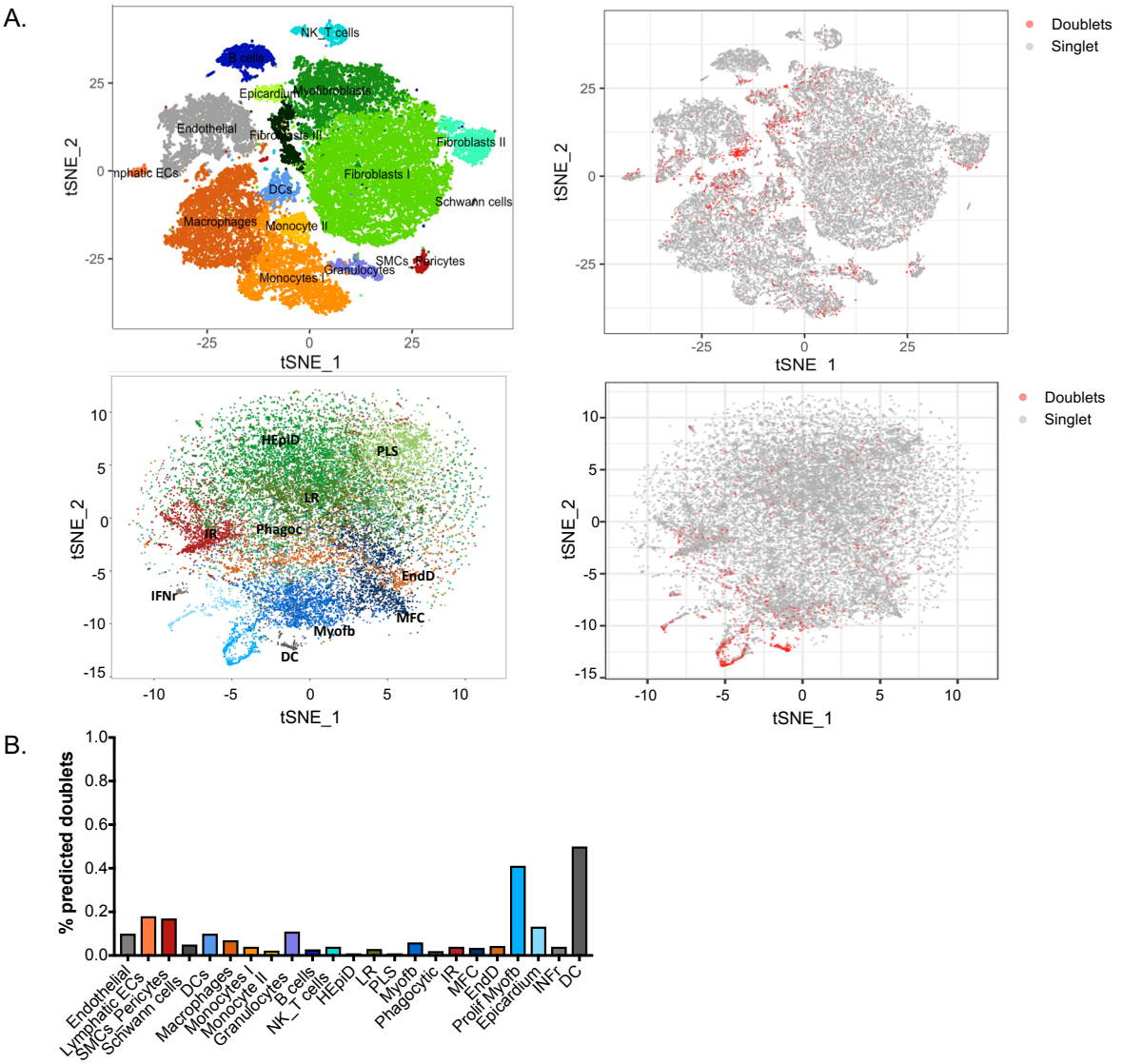

Figure S3 Doublets prediction using DoubletFinder. Related to Figures 1-2. (*A*) tSNE plots representing the distribution of predicted doublets (red on grey) across clusters (first row) and stromal cell sub-clusters (second row). (*B*) Bar plot showing the percentage of predicted doublets in each cluster/sub-cluster.

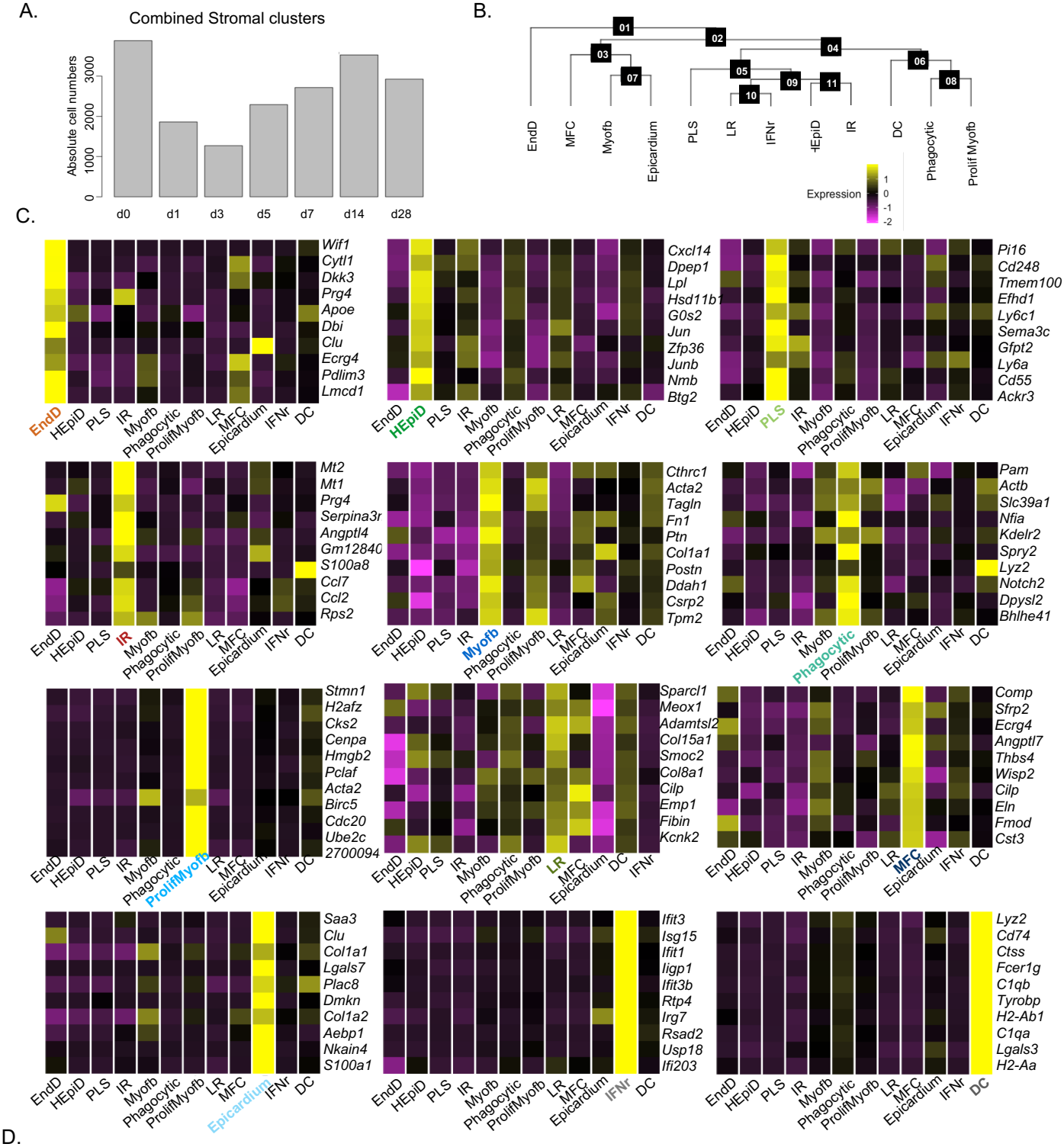

D.

Acromym	Extended name	Notes	Similar population
HEpiD	Homeostatic Epicardial-Derived	Epicardial derived fibroblats prevalent at homeostasis	Fibro Sca Low (F-SL, Farbehi et al 2019)
LR	Late Response Fibroblasts	Epicardial derived fibroblast prevalent in late stage of remodelling.	Fibro Activated (F-Act)
PLS	Progenitor-Like State	Epicardial derived fibroblast expressing higher level of *Ly6a* (progenitor cell markers)	Fibro Sca high (F-SH, Farbehi et al 2019)
Myofb	Myofibroblasts	Specialized fibroblasts, which appear post-injury, capable of contracting and producing producing high quantity of ECM, essential for the closure and stabilization of the injury site	
Phagocytic	Phagocytic	Epicardial derived fibroblasts/myofibroblasts expressing high levels of catalytic enzymes	
IR	Injury Response	Pro-inflammatory, pro-survival gene signature activated soon after injury	
MFC	Matrifibrocytes	Elongated, quiescent, myofibroblasts-derived cells, embedded in the mature scar, which have lost the expression of the contractile protein ACTA2 and produce a more stable, chondrogenic-like ECM	Matrifibrocytes (Fu et al, 2018) IHC, bulk RNAseq
EndD	Endocardial Derived	Endocardial derived fibroblast	Wnt-Expressing (Wnt-X, Farbehi et al 2019); Fibroblasts 2 (Skelly et al, 2018)
Prolif Myofb	Proliferating Myofibroblasts	Myofibroblasts-like cells expressing high levels of cell cycle related genes	Fibroblast-cycling (F-Cyc, Farbehi et al 2019)
Epicardium	Epicardium	Mesothelium surrounding the heart, activated post-injury	
INFr	Interferon-responsive fibroblasts	ZsGreen+ fibroblasts with an interferon response gene signature	Fibroblast: Interferon stimulated (F-IFNS, Farbehi et al 2019)

Figure S4 Detailed analysis of stromal cell sub-populations evolving during the MI repair process. Related to Figures 2-5. (A) Total number of cells from the stromal clusters aggregate (Fibroblasts I, II, III, Myofibroblasts, Epicardium) per time-point used for further sub-clustering with Seurat. (B) Transcriptome based phylogenetic tree of the 11 stromal cell sub-clusters (PC=20, res=0.5). Note EndD cluster node diverges from all epicardial-derived clusters. (C) Heatmaps of the top 10 differentially expressed genes per sub-cluster sorted based on average expression fold change, percentage of expression and adjusted p-value. (D) Nomenclature table explaining the names attributed to each sub-population and how they relate with previous literature.

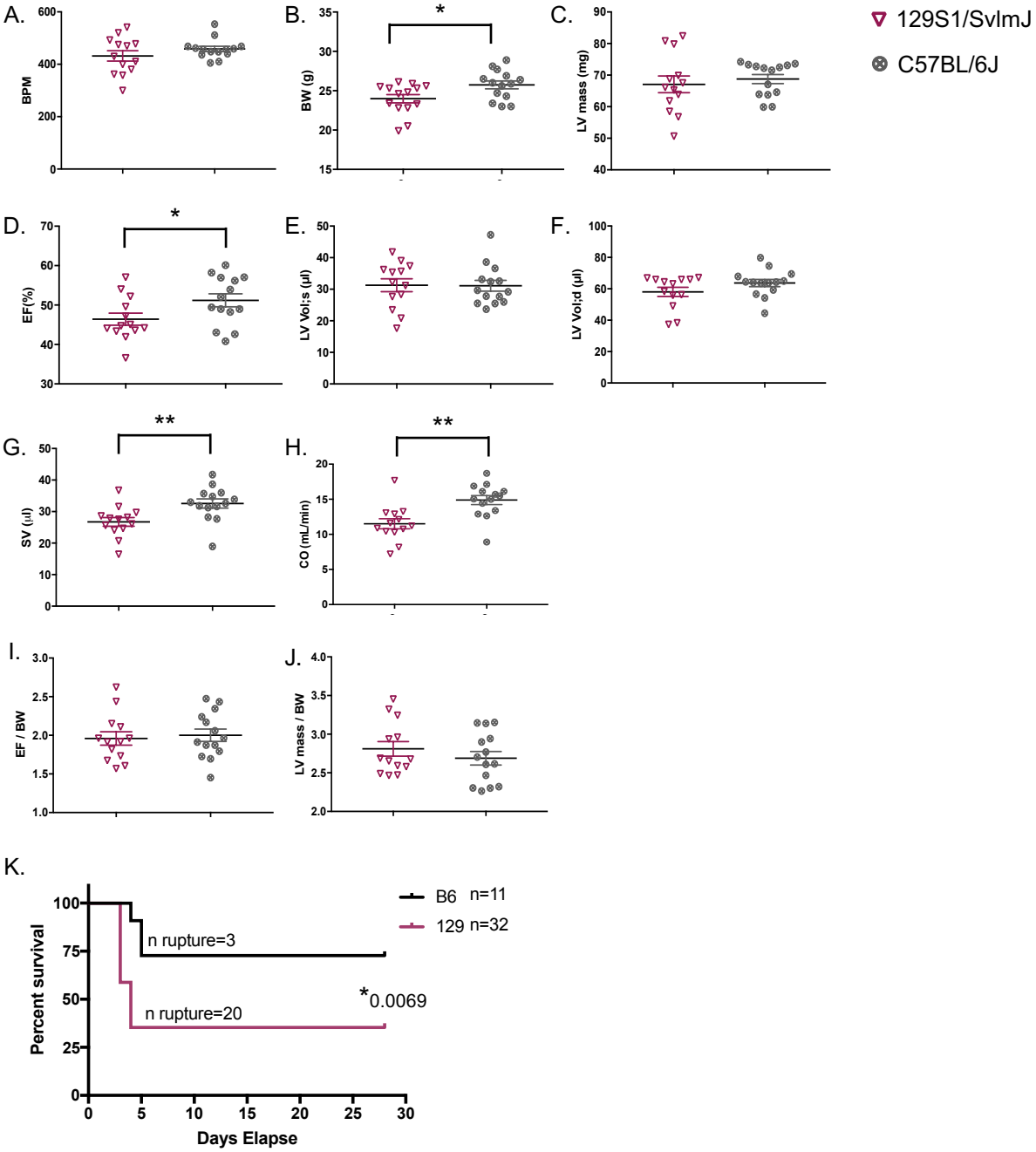

Figure S5 Baseline cardiovascular function in 129S1/SvlmJ and C57BL/6J strains before MI. Related to Figure 6. Echocardiography was performed in 10-week-old 129 (n=13) or B6J (n=14) adult males. Heart rate range ((A) beats per minute or BMP) was controlled between strains for standardization of heart function. 129 showed slightly lower body weight ((B) BW; $p<0.05$), left ventricular mass ((C) LV mass; non-significant), ejection fraction ((D) EF; $p<0.05$), left ventricular diastolic volume ((F), LV Vol;d; non-significant), stroke volume ((G), SV; $p<0.01$) and cardiac output ((H) CO; $p<0.01$) when compared with B6J. Left ventricular systolic volume ((E) LV Vol;s; non-significant) was unaltered. EF and LV mass differences were not significant when normalized by BW (I, J). (K) Kaplan-Meier survival plot for 129 (n=32) and B6J mice (n=11). Two animals for each strain, which were lost to sudden death, were excluded from this analysis. Statistical significance was calculated using the Gehan-Breslow-Wilcoxon test.

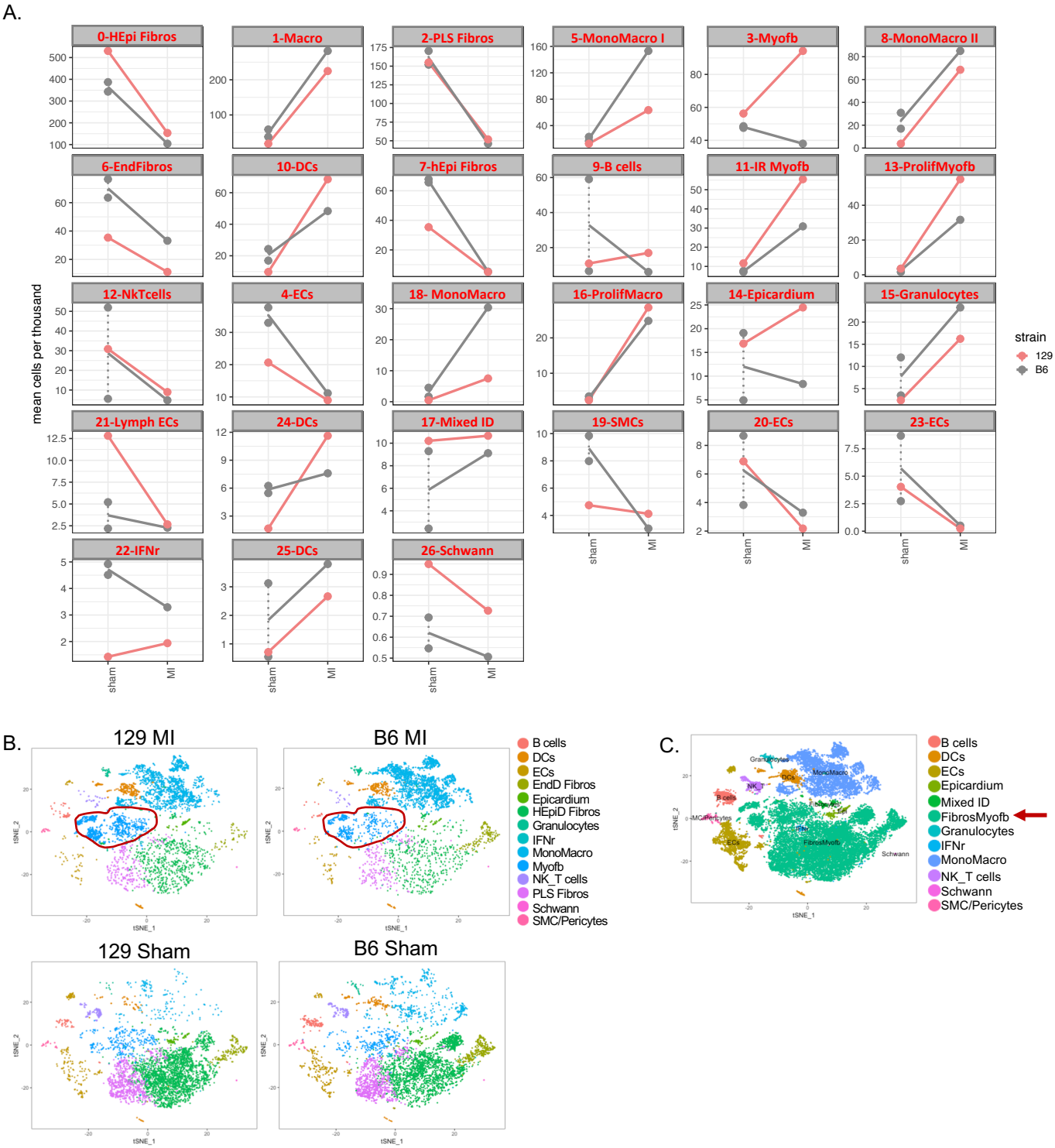

Figure S6 Differential scRNAseq expression analyses between sham and 3d post-MI 129S1/SvImJ and C57bl/6J strains. Related to Figure 6. (*A*) Differential cell composition between sham and 3d post-MI (time-point pre-cardiac rupture) hearts of the two strains. 27 clusters were identified from the analysis of about 17000 cells from 5 samples. The algorithm Harmony was used for the integration of samples from different experiments and genetic backgrounds. (*B*) tSNE visualization of differential cell composition among 129 and B6J sham and 3 days post-MI. Myofb blue cluster (highlighted in red) shows differential cell number between strains (as seen in (*A*)). (*C*) tSNE plot shows the aggregate of stromal cells (fibroblasts and myofibroblasts; red arrow) used for subsequent differential gene expression analysis.

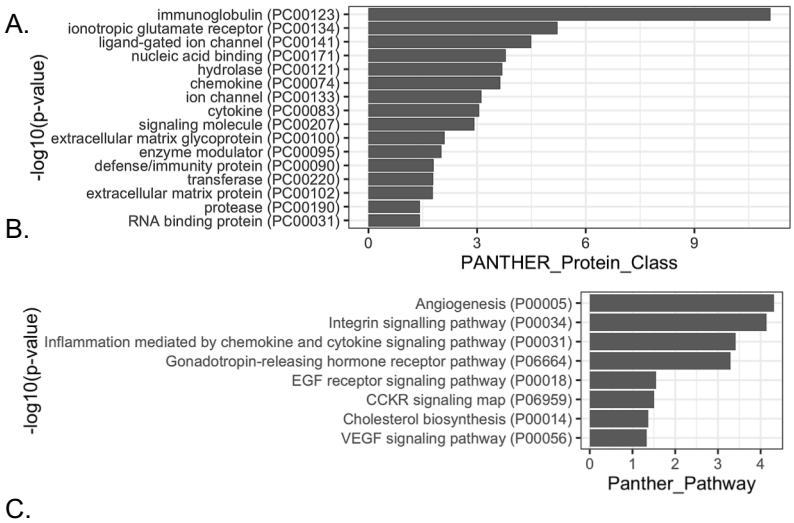

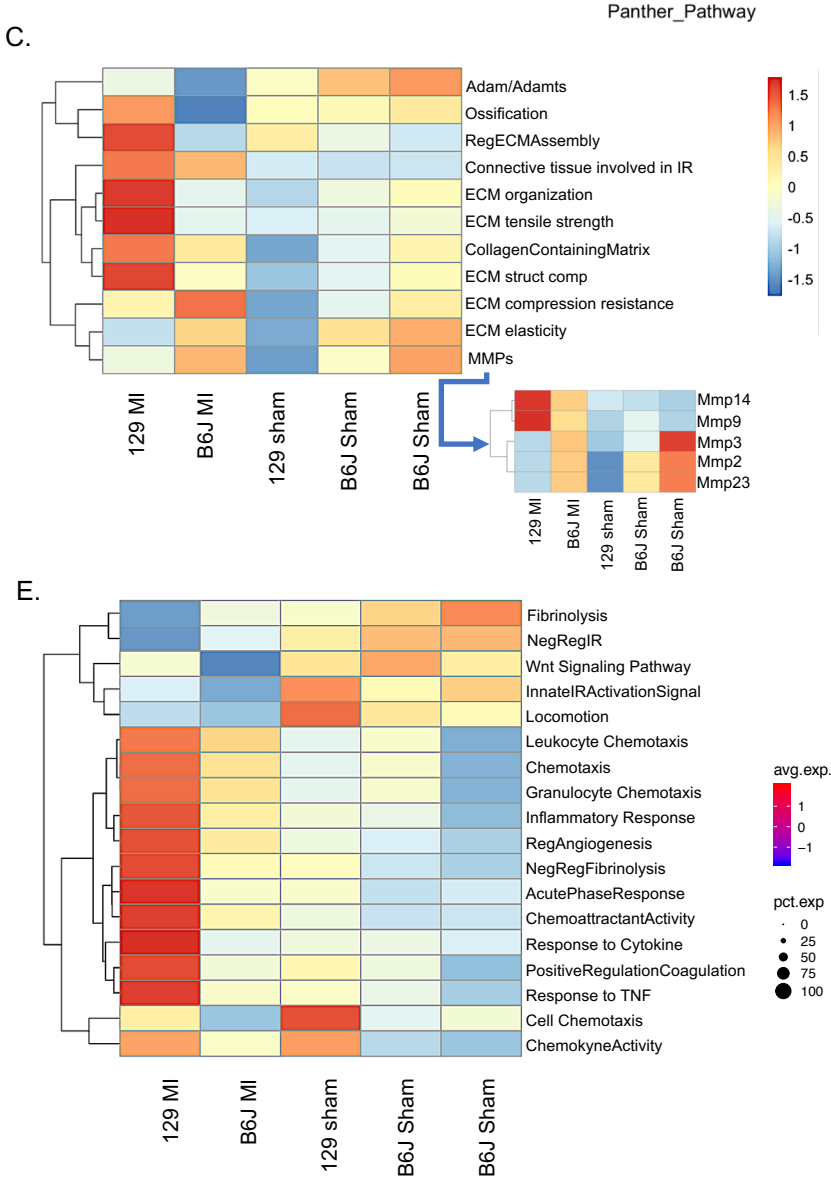

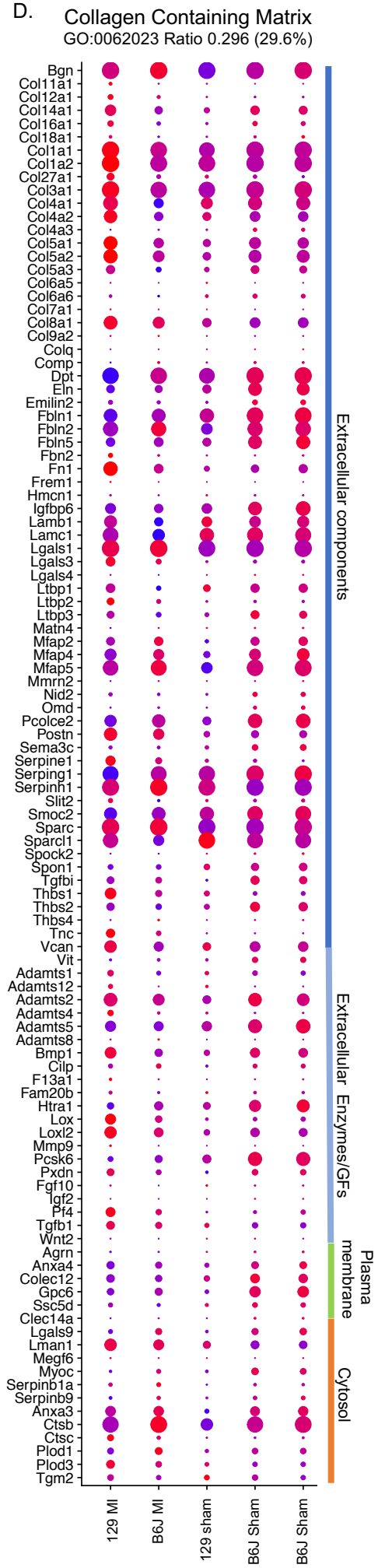

Figure S7 PANTHER and Gene Ontology (GO) analyses of differentially expressed genes between 129 and B6J (sham or d3 post-MI). Related to Figure 7. (*A, B*) Bar plots showing protein classes and pathways respectively, ordered by false discovery rate (FDR)-corrected p-value. (*C, D*), Heatmaps of ECM and injury-response related GO terms, showing the sum of the expression value of all the genes within each term per sample. (*E*) Dot plot showing percentage and intensity of expression of genes within the collagen containing matrix term (GO:0062023). Genes were ordered based on cellular localization and function.

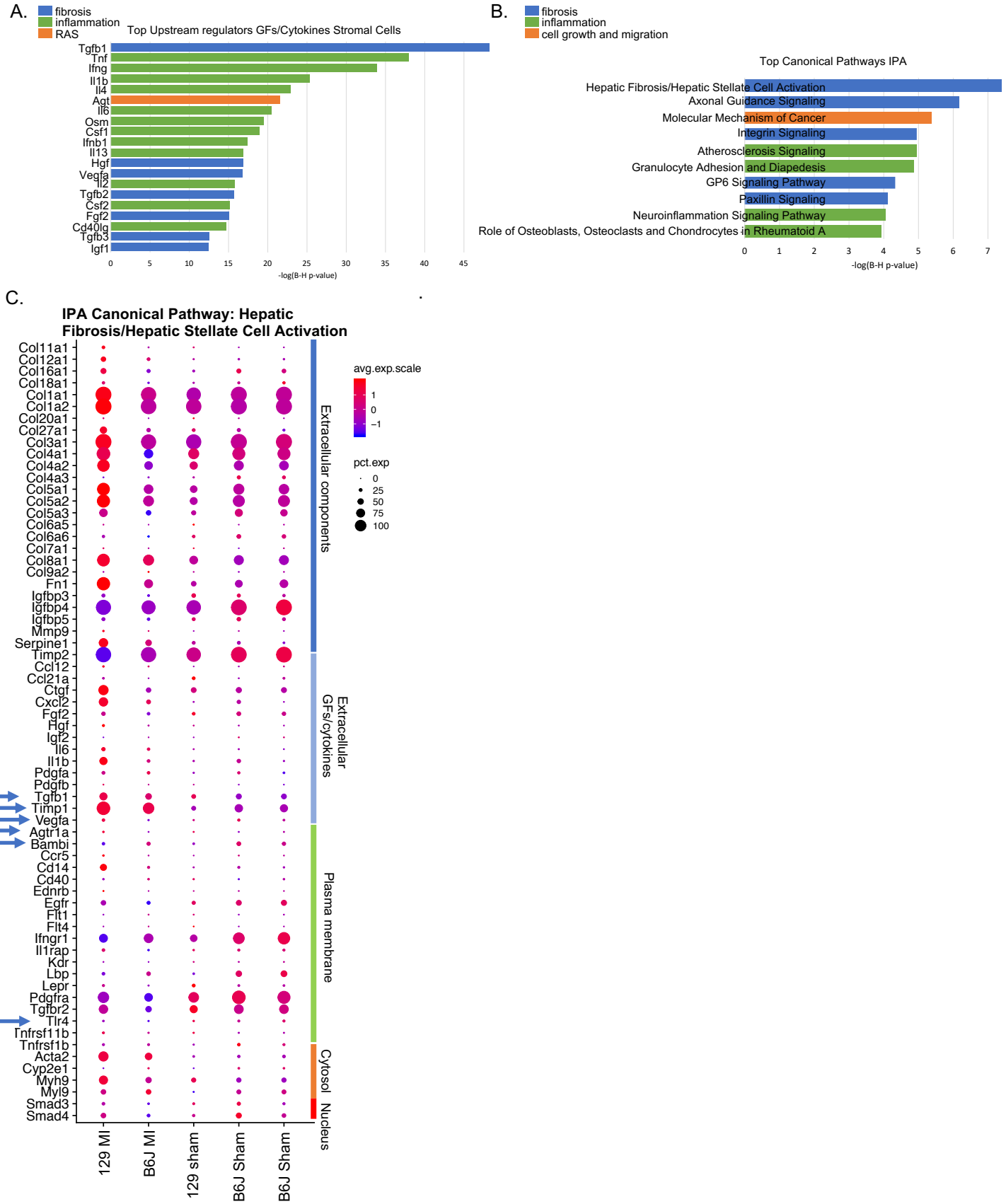

Figure S8 Ingenuity Pathway Analysis (IPA) reveals genes and pathways involved in differential regulation of fibrosis between 129 and B6J mice. Related to Figure 7. 3,922 genes differentially expressed between 129 and B6J (sham or d3 post-MI) were used for analysis. Benjamini-Hochberg (B-H) correction was used for false discovery rate (FDR). (*A*) Bar plot showing the top 20 growth factors and cytokines predicted as upstream regulators of differentially expressed genes, color coded for involvement in fibrosis, inflammation or the renin-angiotensin signaling (RAS) pathway. (*B*) Bar plot showing the top 10 IPA Canonical Pathways, colored by processes related to fibrosis, inflammation or cell growth and migration. (*C*) Dot plot showing the percentage and intensity of expression, across the samples, of genes within the top represented canonical pathway "Hepatic Fibrosis/Hepatic Stellate Cell Activation". Genes were ordered based on cellular location. Blue arrows denote genes involved in the RAS-related pro-fibrotic mechanism.

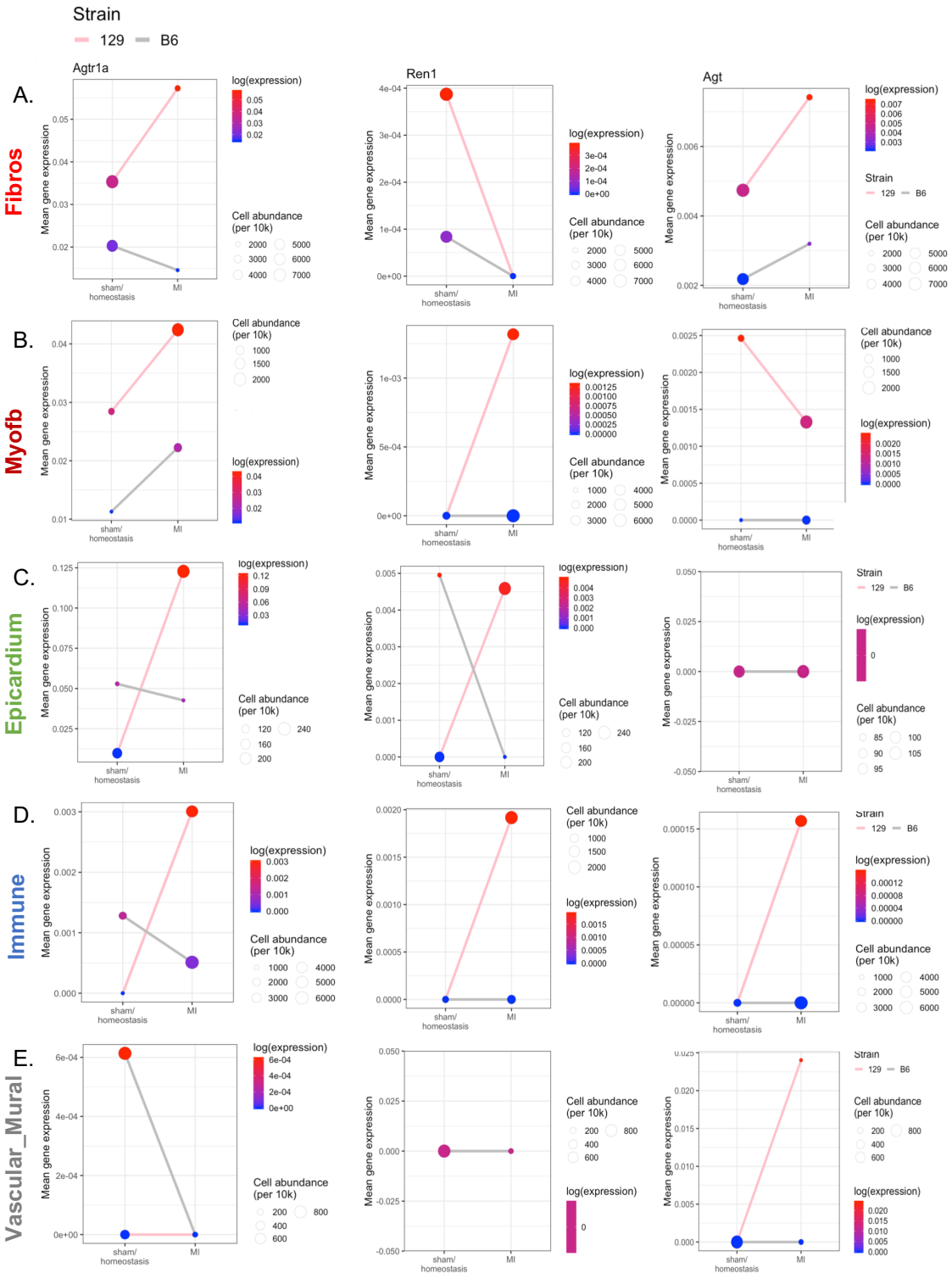

Figure S9 Differential expression of RAS components among diverse cell clusters between 129 and B6J. Related to Figure 7. Dot plots for cell abundance and expression level per each strain and time-point on clusters based on lineage [i.e. fibroblasts (*A*), myofibroblasts (*B*), epicardium (*C*), immune cells (*D*) and vascular mural cells (*E*)] for RAS pathway genes *Agtr1a, Ren1, Agt*.